# Facile preparation of hierarchical nanostructured $CuInS_2$ counter electrodes for dye-sensitized solar cells

**C. Ravi Dhas[1*], A. Jennifer Christy[1], R.Venkatesh[1], S.Esther Santhoshi Monica[1], Subhendu K. Panda[2], B. Subramanian[2], K.Ravichandran[3], P.Sudhagar[4], A. Moses Ezhil Raj[5]**

[1]PG & Research Department of Physics, Bishop Heber College (Autonomous), Tiruchirappalli-620 017, Tamil Nadu, India

[2]CSIR-Central Electrochemical Research Institute (CECRI), Karaikudi-630 006, India

[3]Department of Physics, AVVM Sri Pushpam College, (Autonomous), Poondi, Thanjavur-613 503, Tamil Nadu, India

[4]Department of Materials Engineering, Swansea University, Swansea SA1 8EN, United Kingdom

[5]Department of Physics, Scott Christian College, (Autonomous), Nagercoil-629 003, Tamil Nadu, India

*Corresponding author email address: ravidhasc@gmail.com

**Corresponding Author**

**Dr.C. Ravi Dhas**
Assistant Professor and Head,
PG & Research Department of Physics,
Bishop Heber College (Autonomous),
Tiruchirappalli-620 017, Tamil Nadu, India.
Mobile: +91 9443076209
Land line: 0431-2770136
Fax: 0431-2770293
e-mail: ravidhasc@gmail.com; cravidhas@gmail.com

**Abstract**

$CuInS_2$ (CIS) thin films have been synthesized onto the glass substrates for different solvent volumes (10, 30, 50 and 70 ml) by nebulizer spray technique. The effect of solvent volume on the structural, morphological, compositional, optical and electrical properties of CIS thin films has been investigated. X-ray diffraction patterns suggest that the obtained CIS films are polycrystalline with the tetragonal structure. The surface morphology of the prepared CIS films purely depends on the solvent volume. The elemental quantitative investigation and the stoichiometric ratio of the CIS thin films were verified from XPS and EDS. High absorbance with the optical band gap of 1.13 eV was obtained at the higher solvent volume. All the deposited CIS thin films exhibited p-type semiconducting behavior with the high electrical conductivity and carrier concentration. CIS thin films deposited onto the FTO substrate were used as a counter electrode (CE) in dye-sensitized solar cells. CIS CEs possessed high electrocatalytic behavior and fast electron charge transfer at the CE/electrolyte interface. The CIS CE prepared using 50 ml solvent volume generated high energy conversion efficiency of about 3.25 %.

**Keywords:** Copper indium sulphide, nebulizer spray, counter electrode

## 1. Introduction

The increase in global warming, emissions of greenhouse gases from fossil fuels and global population, etc is the major motivation behind the development of low-cost photovoltaic devices which can generate more photons and achieve the maximum power conversion efficiency under sun light [1]. Dye-sensitized solar cells (DSSCs) that belong to third generation solar cell, are widely used for photoenergy conversion due to their low-cost, large scale production, environmental friendliness, etc. [2-4]. Generally, DSSC consists of

dye-absorbed photoanode $TiO_2$ coated on FTO, an electrolyte with $I^-/I_3^-$ and a counter electrode (CE) [5]. The CE plays a vital role in DSSC as it collects electron from the external circuit and reduces the redox species ($I^-/I_3^-$) in the electrolyte. The CE material should possess high electrocatalytic activity, good stability, and high electrical conductivity [6]. Platinum (Pt) is widely used as a CE because of its high electrocatalytic activity and electrical conductivity. Since Pt is a noble metal, its expensiveness restricts large scale production. Therefore, an alternative material with good mechanical and chemical stability should substitute the Pt CE. Carbon-based materials [7], conducting polymers [8], metallic nanomaterials [9-11], etc are mostly used in the place of Pt CE in DSSC devices.

In recent days, transition metal sulfides have been paid more attention as they have unique catalytic and electrical activities [12]. Among ternary multi-metal sulfide, copper indium disulfide (CIS) is one of the promising candidates as a light absorber or counter electrode in DSSCs owing to its being inexpensive and ease of fabrication [13]. $CuInS_2$ thin film exhibits high absorption co-efficient of about $10^5$ $cm^{-1}$ in the visible region with the optical band gap lying between 1.1 and 1.5 eV and good chemical stability [14]. CIS CE has been prepared by various techniques like SILAR, hydrothermal, solvothermal, spin coating, etc followed by annealing under inert/$H_2S$ atmosphere [13, 15-17]. So far there have been no reports available for CIS CE prepared by spray pyrolysis to the best of our knowledge. Nebulizer spray technique is more advanced, simple and cost effective method compared to conventional chemical spray pyrolysis technique for the production of uniform and adherent coatings on large scale [18]. Other merits in utilizing nebulizer spray deposition process are: (i) straight forward approach or no post thermal treatment required (ii) device quality films can be achieved even at lower temperatures, and (iii) stoichiometry of the films can be controlled easily. In this present report, we made an attempt to study the influence of solvent

volume on physical properties and electrocatalytic performance of nebulizer spray-coated CIS thin films as CE in DSSCs.

## 2. Experimental

### *2.1 Preparation of CIS thin film*

The functioning of nebulizer spray technique has been discussed in the previous paper [19]. The sources of copper, indium and sulfur were copper Chloride ($CuCl_2$), indium chloride ($InCl_3$), and thiourea $SC(NH_2)_2$ respectively (molar ratio of 1:1:4), purchased from Alfa Aesar (AR grade-99.99%) and were used without further purification. De-ionized water was used as a solvent for $CuCl_2$, $InCl_3$, and SC $(NH_2)_2$, under vigorous stirring at room temperature. The solution thus prepared was sprayed over the substrates (glass and FTO) at 300 ℃ for different solvent volumes (10, 30, 50 and 70 ml) to grow CIS thin films.

### *2.2. Fabrication of DSSCs device*

Spin coating method was used for the preparation of blocking layer ($TiO_2$) film using $TiCl_4$ and was annealed at 450 °C for 30 minutes. For the preparation of 21 nm mesoporous $TiO_2$ layer and 150 nm $TiO_2$ scattering layer, doctor blade method was employed and the films were annealed at 150 °C for 5 minutes and 500 °C for 1 hour respectively. The films were further dipped into the ethanolic solution of N719 (di-tetra-butyl ammonium *cis*-bis (isothiocyanato) bis (2,2′-bipyridyl-4,4′-dicarboxylato) ruthenium (II)) for 12 hours at ambient condition. The excess of dye molecules present on the $TiO_2$ film was cleansed with ethanol and allowed to dry. On the other hand, Platinum (Pt)-coated FTO CE was prepared by spin coating method using isopropanol solution of $H_2PtCl_6.6H_2O$. It was annealed at 400 °C for 30 minutes and taken for comparison. The prepared CIS/FTO CEs were sandwiched with dye-sensitized $TiO_2$ using surlyn film to form DSSC with an active area of 0.4 × 0.4

$cm^2$. The liquid electrolyte containing 0.03 M $I_2$, 0.06 M LiI, 0.5 M 4-tert-butyl pyridine, 0.6 M 1-propyl-2,3-dimethylimidazolium iodide and 0.1 M guanidinium thiocyanate was injected between electrodes for the study of photocurrent density – voltage.

*2.3. Characterization*

The X-ray diffraction spectra were analyzed with a PANanalytical X'PERT PRO diffractometer using the Cu $K_\alpha$ rays at the wavelength of 1.54 Å. Raman analysis was carried out by Raman spectrometer (Reinshaw Invia Make). Scanning electron microscope (VEGA3 TESCAN) and Atomic force microscope (A100, APE Research) were used to analyze the surface morphology of the film. X-ray photoelectron spectroscopy (Kratos Axis Ultra DLD) was employed to study the chemical state of the CIS thin film and its composition were observed using Energy dispersive X-ray analysis spectra (Bruker). The optical characterization was recorded using JASCO UV-Vis-NIR-V-670 spectrophotometer. The investigation of Hall and Electrical measurements were achieved by four probe method using Ecopia HMS-3000 Hall measurement system and Keithley 2400 source meter respectively. A potentiostat (VMP3, BIO-LOGIC) was used for the measurement of photocurrent density – voltage of the prepared DSSCs under Solar Simulator (Photoemission Tech) having AM 1.5G filter set and 100 $mW/cm^2$ intensity. A three electrode cell setup was used in electrochemical experiments. Cyclic voltammetry studies were conducted at a scan rate of 50 mV/s in electrolyte solution consist of 10 mM LiI, 1mM $I_2$, and 0.1 M $LiClO_4$ dissolved in acetonirile. Pt wire, standard calomel electrode (SCE) and CIS/FTO were used as counter electrode, reference electrode and working electrode respectively.

## 3. Results and Discussion

### *3.1. Thickness measurement*

The variation of film thickness deposited for different solvent volumes is shown in Fig. 1. The thickness of the film was recorded by stylus profilometer and varies between 300-1320 nm for different solvent volumes. That the increase in film thickness was not exactly proportional to the increase in solvent volume could be attributed to gas convection, driving the droplets of the solvent aside as it reduces the mass transport to the substrate [20]. Apparently, the thickness of the film decreased for the film coated using 70 ml. This is due to the fact that the ability of atomizer restricts the yield of the process and hence large amount of energy is required for higher concentrations to stimulate the spray process [21].

### *3.2. Structural analysis*

X-ray diffraction (XRD) spectra of CIS thin films deposited for different solvent volumes are shown in Fig. 2. The peaks obtained at (2θ) 27.6 °, 46.4 ° and 54.9 ° were assigned to (1 1 2), (2 0 4) and (2 1 5) planes respectively and in agreement with the tetragonal structure of $CuInS_2$ (JCPDS card no. 65-1572). The plane (1 1 2) grows preferentially with increase in solvent volume as it has the lowest surface energy [22]. The intensity of the planes increases gradually with the increasing solvent volume upto 50 ml due to the growth of large crystallites as it is directly proportional to concentration of the solute and possessed better crystallinity [20]. The preferential orientation in a chalcopyrite film promotes faster electron transport and thereby enhancing higher electrocatalytic behavior [23]. The peak intensity decreases for the film prepared using higher solvent volume as the higher impinging rate of precursor species over the substrate leads to incomplete pyrolytic decomposition [24].

The crystallite size of the CIS thin films for the plane (1 1 2) was estimated from Scherrer formula [25]

$$D = \frac{K\,\lambda}{\beta \cos\theta} \qquad (1)$$

where 'D' is the crystallite size (nm), 'K' = 0.9 is the shape factor, 'λ' is the wavelength of X-ray (Kα=1.5406 Å), 'β' is the full-width half maximum, 'θ' is the diffraction angle. From Fig. 3, it is noted that the crystallite size increases monotonously with the increasing film thickness and beyond 70 ml, the crystallite size decreases. The reason behind the rise in crystallite size upto 50 ml solvent volume is the sufficient amount of time and required amount of solute atoms is available to undergo electrostatic interaction and results in the formation of larger crystallite size [26, 27]. The tiny crystallites on the substrate are unable to develop into large crystallites as they are deposited for short duration of time, and hence the film deposited at lower solvent volume has smaller crystallites than the film deposited at higher solvent volume. The decline in crystallite size is provoked by the structural defects and lattice distortion for the film deposited at 70 ml.

The microstrain (ε) and dislocation density (δ) of the CIS thin films were calculated by the following relation,

$$\varepsilon = \frac{\beta \cos\theta}{4} \qquad (2)$$

$$\delta = \frac{1}{D^2} \qquad (3)$$

The increase in crystallite size and corresponding decrement in strain and dislocation density with increase in film thickness (Fig. 3) are an indication of the decrease in structural defects and release of intrinsic stress developed at the grain boundaries [28].

Raman spectroscopy is used to examine the vibrational modes of the film surface. As reported in the previous paper [29], CIS thin film has two structures CH- ordering and CA-ordering. Figure 4 clearly depicted that the peak shifted with the increase in the solvent volumes. A peak appeared at 304 and 302 $cm^{-1}$ ($A_1$ mode) corresponding to the solvent volumes of 10 and 30 ml indicating that CA-structure could be attributed to ordered vacancy compounds [30]. The peak shift observed for $A_1$ mode could be due to the morphological or thickness variation with increase in solvent volume [30]. As the solvent volume increases, the peak shifted to lower wavenumber region 299 and 297 $cm^{-1}$ indicating the combination of both the structures. The FWHM value was determined to be 34.8, 32.9, 32.5 and 33.2 $cm^{-1}$ with the increment in the solvent volume. The lowest FWHM value obtained for the solvent volume 50 ml enhanced the better crystallinity in the film and promotes higher efficiency in DSSCs as witnessed from XRD results.

*3.2. Surface morphology analysis*

The surface morphology of the nebulizer spray-coated CIS thin films was analyzed by scanning electron microscope (SEM) and atomic force microscope (AFM). The SEM images of CIS thin film deposited for different solvent volumes are shown in Fig. 5. Tiny needle-like-shaped grains were observed for the CIS thin films prepared using low solvent volume (10 & 30 ml). As the preferential orientation plane (1 1 2) begins to emerge with the increase in solvent volume (50 ml), this needle-like-shape turned into nanorod morphology. Figure 5 (v) shows higher magnification of CIS thin film deposited by 50ml. According to the Van der Drift model, the random orientation nuclei were formed at the beginning stage of deposition

and then the nanorod-like structures were developed for the CIS film deposited by 50 ml [31]. The hierarchical nanorod structure offers enormous channels to transfer the charge carriers from their surface to the conducting FTO substrate, and henceforth improving the electrocatalytic activity of CIS films [23]. At the higher solvent volume (70 ml), the agglomeration occurs due to coalescence of larger particles [32].

Figure 6 shows the AFM micrographs of the CIS thin film prepared for different solvent volumes. The grains are non-homogeneously distributed over the surface of the CIS film deposited by the lower solvent volume (10 and 30 ml) that led to large surface roughness. The uniform growth of grains was observed for the CIS thin film prepared using 50 ml. The grain growth mainly depends on the nucleation density and re-crystallization and hence larger grains restrict the surface defects and enhances the crystallinity of the CIS thin film which is more beneficial to dye-sensitized solar cells [33]. The surface roughness of the CIS thin film observed to be decreased with increasing solvent volume. According to Moholkar et al. [34], the decrease in surface roughness with the increasing thickness could be due to the time involved in the deposition as the ad-atoms gained sufficient thermal energy to get settled at the suitable lattice position. In our present case the deposition time gets increased by increasing the solvent volume and therefore the above discussion supports our roughness values. The grains of the CIS thin film deposited at the higher solvent volume 70 ml were found to be agglomerated resulting in an increase in surface roughness due to the slow spreading of the rich solute [35].

*3.3. Compositional analysis*

The energy dispersive X-ray analysis spectra of CIS thin film coated for 50 ml solvent volume is shown in Fig. 7. Copper, indium and sulfur were the only elements present in the

prepared film confirming its purity. The inset of the table in Fig. 7 represents the better stoichiometric ratio attained for the CIS thin film deposited using different solvent volumes.

The chemical state of the elements present in the CIS thin film deposited for the solvent volume of 50 ml was investigated by XPS. Carbon species C 1s (284.6 eV) arises from the mesh employed for analysis and used to calibrate the binding energies of other elements present in the deposited CIS film. Figure 8 shows the survey spectrum of CIS thin film analyzed in the binding energy range between 0 – 1200 eV. The survey spectrum clearly depicts copper, indium and sulfur. No significant presence of impurities was observed in the film other than little amounts of carbon and oxygen. The oxygen O 1s (531.2 eV) is expected as the film was being prepared in the open atmosphere. The obtained binding energy values of Cu 2p, In 3d and S 2p for CIS film deposited by nebulized spray technique are supported by previous literature [36]. Zouaghi et al. [37] reported chlorine peak around 198 – 200 eV in the spray-deposited CIS film, whereas that peak is not observed in our spectrum. This confirms the purity of $CuInS_2$ phase as evident from XRD and Raman studies.

The core level spectrum of copper has two peaks at 931.3 and 951.1 eV assigned to Cu $2p_{3/2}$ and Cu $2p_{1/2}$. The two peaks split with an energy difference of 19.8 eV, in good agreement with the Cu (I) oxidation state. Cu (II) state is an indicative of peak at 942 eV not observed in the core level spectrum and signifies that no other phases like $Cu_xS$ are present [38]. The indium peaks with the splitting of binding energy 7.6 eV centred at 444.0 and 451.6 eV correspond to In (III) state of $3d_{5/2}$ and $3d_{3/2}$ respectively. A peak located at 161.2 and 167.9 eV is attributed to sulfides and sulfates representing S 2p state in the spectrum [39].

*3.4. Electrical studies*

The electrical parameters of CIS thin film play an important role in determining the electrocatalytic activity of counter electrodes in DSSC. Figure 9 shows the dependence of solvent volume over carrier concentration, mobility and resistivity of the prepared CIS films. The measurements were made at room temperature under Van der Pauw configuration. CIS films prepared by different solvent volumes exhibited p-type semiconducting behaviour. The obtained carrier concentration values are $4.47\times10^{18}$, $8.54\times10^{19}$ $1.08\times10^{20}$, $1.44\times10^{19}$ $cm^{-3}$ for the films deposited using 10, 30, 50 and 70 ml respectively. The hole mobility values lie in the range between 1.26 and 62 $cm^2/Vs$. The obtained carrier concentration and mobility values are supported by previously reported literatures [40, 41]. The carrier concentration increases monotonously with the increase in solvent volume upto 50 ml. The decrease in carrier concentration value for 70 ml could be attributed to the defects and lattice distortion as discussed from XRD results. The variation in carrier concentration and mobility values observed from Hall measurements can be correlated with different possibilities such as scattering of charge carriers at the grain boundaries, deviations in stoichiometry and crystalline quality.

According to the theory of band conduction model, in a polycrystalline semiconductor thin film, the grain boundary effect on electrical carriers can be assessed by estimation of the Debye screening length ($L_D$) [42]:

$$L_D = \sqrt{\left(\frac{\varepsilon\varepsilon_0 kT}{e^2 N_D}\right)} \qquad (4)$$

where 'ε' is the specific dielectric constant of $CuInS_2$ films [43]. '$\varepsilon_0$' is dielectric constant in vacuum, 'k' is the Boltzmann constant and '$N_D$' denotes the hole concentration of the films. The obtained Debye screening length ($L_D$) values are $1.81\times10^{-6}$, $4.15\times10^{-6}$, $3.69\times10^{-7}$,

$1.02\times10^{-6}$ m for CIS films deposited using 10, 30, 50 and 70 ml respectively. The estimated crystallite size from X-ray diffraction values lies in the range of $10^{-9}$ m and hence the relation $L_D > D$ holds good and indicates that no grain boundary scattering results in better charge transport. The change in carrier concentration and mobility values with the solvent volume does not arise due to the grain boundary scattering but only due to a small deviations as observed from EDS results which is proposed by Sankir et al. [40].

Figure 10 shows the Arrhenius plot representing the non-linear semiconducting behaviour with the absolute temperature. Two different activation energies ($E_a$I and $E_a$II) were determined from slopes of two different regions (region I: 303-383 K and region II: 383-453 K). The obtained activation energy values are listed in Table 1. The activation energy $E_{aI}$ is attributed to variable range hopping conduction (VRH) and $E_{aII}$ due to thermionic emission of carriers. The reduced activation energy values observed with increasing solvent volume were owed to decrease in defect density of polycrystalline CIS films.

*3.5. Optical properties*

The absorbance spectra of CIS thin films prepared for different solvent volumes are recorded in the wavelength range of 300 -1800 nm at room temperature and shown in Fig. 11. All the CIS thin films exhibited high absorbance in the UV-Vis region [44]. Wide absorption spectra in the visible region promote high efficiency in the solar cell applications. The broad and maximum absorbance was attained for the CIS film deposited using 50 ml solution compared to the other conditions. This could be attributed to the higher thickness of the film and hence the thickness of the CIS thin film plays a crucial role.

Using the Tauc plot relation (Eq.5), the optical band gap energy of the CIS thin film can be analyzed [25].

$$\alpha h\nu = A\left(h\nu - E_g\right)^n \quad (5)$$

where 'α'indicates the absorption co-efficient, 'hν' is the incident photon energy, '$E_g$' represents the band gap and 'n' denotes the type of transition. Since CIS is a direct band gap semiconducting material, the value of 'n' is assumed to be 1/2 [45]. By extrapolating tangents to the 'x'-axis, the optical band gap energy values are determined to be 1.72, 1.37, 1.13, and 1.27 eV with the increasing solvent volume (Fig. 12). The band gap value of CIS thin film decreased with the increase in film thickness which might be due to the reduction in microstrain and native defects results in increase of density of localized states in the band gap [14].

*3.6. Electrochemical properties*

The electrocatalytic activity of CIS and Pt counter electrodes (CEs) was studied using cyclic voltammetry (CV), electrochemical impedance (EIS) and Tafel polarization measurements in the tri-iodide electrolyte. Figure 13 (i) represents the CIS CEs having excellent electrochemical activity in $I^-/I_3^-$ reactions. A pair of oxidation and reduction peaks was observed in the CV studies for all the CIS CEs.

$$3I^- \leftrightarrow I_3^- + 2e^- \quad (6)$$

The anodic ($J_{pa}$) and cathodic ($J_{pc}$) peak current densities and peak-to-peak separation ($\Delta E_p$) are the two vital parameters to determine the catalytic activities [46] and the values are listed in Table 2. The thickness of the CIS CEs has no effect on the cathodic potential but the cathodic peak current density increases with the solvent volume. The highest $J_{pc}$ and the

lowest $\Delta E_p$ were obtained for the CIS CE deposited by 50 ml implying better electrocatalytic activity towards the oxidation and reduction of ($I^-/I_3^-$) couple. Highly oriented (1 1 2) plane with nanorod morphology and greater carrier density observed for CIS CE (50 ml) provides more efficient pathways for charge transport and results in better electrocatalytic activity. With further increase in the solvent volume (70 ml), the $J_{pc}$ value decreased with an increase in $\Delta E_p$ indicating that the thickness of the CIS CE plays an important activity in the redox couple process. Stability assessment of the counter electrode is one of the major issues in the fabrication of DSSCs [47]. To confirm the stability of the CIS CE deposited using 50 ml for longer duration, CV was carried out for 40 consecutive cycles in the $I^-/I_3^-$ electrolyte solution. From Fig. 13 (ii), the consistent value of anodic and cathodic peak current densities was obtained. Figure 13 (ii) reveals that the CIS CEs prepared by nebulizer spray are stable in the tri-iodide electrolyte system and can be efficiently used as CE and might replace Pt CE in DSSCs.

The catalytic activity of CIS CEs was further investigated by electrochemical impedance spectroscopy (EIS) in the reduction of $I_3^-$ ions. The EIS analysis of CIS CEs with the $TiO_2$ based-DSSCs devices is shown in Fig. 14 (i). The high-frequency intercepts on the 'x'-axes denote the series resistance ($R_s$), which is a sum of the bulk resistance of CE materials and FTO resistance. The high-frequency semicircle represents the charge transfer resistance ($R_{ct}$) in the CE/electrolyte interface. The Zsimpwin software was used to fit the equivalent circuit of impedance spectra of the CIS CEs as shown in the inset of Fig.14 (i). A fitted graph has been plotted for the counter electrode prepared by 50 ml which is shown in Fig.14 (i). The EIS parameters deduced for CIS CEs are displayed in Table 2. The value of $R_s$ and $R_{ct}$ decreases with the increasing solvent volume of the prepared CIS CEs. The least $R_s$ value of CIS CE deposited by 50 ml reveals a superior bonding strength between the CIS films and FTO substrate which can be witnessed from electrical studies. This led to the

transfer of a large amount of electrons from the external circuit to the CEs [48]. The CIS CE coated for 50 ml solvent volume results in the lowest $R_{ct}$ value that promotes an acceleration of high electron charge transfer at the CE/electrolyte interface and high electrocatalytic activity [23]. The decrement in $R_s$ and $R_{ct}$ values causes an increase in the fill factor and short-circuit current density of the DSSCs [49].

Tafel polarization measurements (log J vs V) were made to understand the electrocatalytic activity of the prepared $CuInS_2$ CEs and compared with the Pt counter electrode. The obtained curves are given in Fig. 14 (ii). The parameters exchange current density ($J_0$) and diffusion coefficient ($J_{lim}$) were deduced from the slope and intercept of Tafel curves. The estimated value of log $J_{lim}$ is listed in Table 2. The CIS film prepared using 50 ml solvent volumes possesses the maximum log $J_0$ and log $J_{lim}$ among the prepared CIS counter electrodes. The decrement in $J_{lim}$ value for the CIS counter electrode prepared by 70 ml could be due to the agglomerated morphology which limits the amount of iodine species diffused into the counter electrode as evident from SEM analysis [50].

*3.7. Photocurrent density-voltage (J-V) characterization*

Figure 15 shows the photocurrent density-voltage (J-V) studies of DSSCs using CIS and Pt CEs evaluated under constant light intensity of 100 $mW/cm^2$. The obtained photovoltaic parameters of DSSCs are listed in Table 3. The variation in solvent volume has a pronounced effect over the crystallite grain boundaries and in turn electrical conduction of the prepared CIS films. The dominant orientation along (1 1 2) plane for CIS thin film with increase in thickness leads to reduction in grain boundary volume. This results in decrease of trapping centers for charge carriers and promotes better charge transport. The minimum value of short-circuit current density ($J_{sc}$) acquired in the lower thickness of the CIS CEs could be attributed to high resistivity and low electrocatalytic activity in the redox couple. The

obtained $J_{sc}$ and $V_{oc}$ values of CEs are in correlation with the electrical conductivity and electrochemical values studied from CV analysis. The short-circuit current density ($J_{sc}$) increases with the increasing solvent volume. The maximum $J_{sc}$ and fill factor (FF) was observed for the CIS CE deposited using 50 ml. The higher value of FF in DSSCs is due to the lower value of $R_s$ as evident from the EIS studies. The efficiency (η) of CIS CE prepared by 50 ml achieved the maximum value of 3.25 % compared to other CIS CEs. With further increase in the solvent volume, the efficiency falls down to 2.52 % with the FF of 0.45 due to the lower carrier concentration and powdery nature of the films. Bhosale et al. have prepared $CuInS_2$ by SILAR technique and achieved a maximum current conversion efficiency of about 5.0 % after post processing thermal treatment at 500 °C under $H_2S$ and Ar atmosphere [15]. Chen et al. have demonstrated a maximum efficiency of about 2.84% for the template assisted as prepared $CuInS_2$ films and observed an improvement in efficiency after annealing at 400 °C [13]. Liu et al. have prepared $CuInS_2$ CEs by solvothermal method annealed at 450 °C in argon environment and obtained a maximum efficiency of about 3.31% [17]. It is noteworthy to mention that we have adopted the single step deposition technique and have not done any post processing thermal treatment under argon/$H_2S$. It can be concluded that nebulizer spray technique is more efficient chemical approach for the synthesis of $CuInS_2$ counter electrodes and by making suitable modifications in deposition parameters Pt electrode could be replaced by $CuInS_2$ CE in future.

## 4. Conclusion

The effect of solvent volume on the physicochemical properties of CIS thin films deposited by nebulizer spray method has been studied. The crystalline quality of CIS thin films enhanced with the increasing solvent volume and exhibited tetragonal structure. The morphology of the CIS thin film deposited using 50 ml was found to be hierarchical nanorod

structure with the minimum surface roughness. The electrical conductivity of CIS thin films with higher carrier concentration was achieved for the thicker films. DSSCs were fabricated with the CIS thin film for different solvent volumes. The CV analysis demonstrated the Pt-like electrocatalytic activity for the deposited CIS films. The minimum $R_s$ and $R_{ct}$ obtained for the CIS CE deposited using 50 ml indicates the enhancement in bonding strength and charge transfer kinetics at the CE/electrolyte interface. The CIS CEs deposited for different solvent volumes affected the photocurrent density and fill factor. The best photo-conversion efficiency of about 3.25 % was obtained for the CIS CE prepared by 50 ml solvent volume. The efficiency of CIS CE could be improved by optimizing the other technical parameters.

**Acknowledgement**

The authors would like to record their sincere thanks to the University Grants Commission, New Delhi for providing financial support through Major Research Project Scheme (MRP) [F.no.42-903/2013(SR)]. The authors also acknowledge Dr. R. Ramesh Babu, Assistant Professor, School of Physics, Bharathidasan University, Tiruchirappalli-24, for extending the Hall measurement facilities established under the DST grant (D.O.No.SR/S2/CMP-35/2004). One of the authors, Dr. S. K. Panda, would like to thank the Department of Science and Technology (DST), Government of India, for the financial support (Project no: SB/FT/CS-048/2012).

**References**


[1] H-J Kim, B Ko, CV Gopi, M Venkata-Haritha, Y-S Lee, 2017 J. Electroanal. Chem. **791**: 95.

[2] Z Zhang, X Zhang, H Xu, Z Liu, S Pang, X Zhou, S Dong, X Chen, G Cui, 2012 ACS applied materials & interfaces **4**: 6242.

[3] L Heng, X Wang, N Yang, J Zhai, M Wan, L Jiang, 2010 Adv. Funct. Mater. **20**: 266.

[4] J Guo, X Wang, W-H Zhou, Z-X Chang, X Wang, Z-J Zhou, S-X Wu, 2013 RSC Advances **3**: 14731.

[5] R Cruz, DAP Tanaka, A Mendes, 2012 Solar Energy **86**: 716.

[6] M Grätzel, 2003 Journal of Photochemistry and Photobiology C: Photochemistry Reviews **4**: 145.

[7] JD Roy-Mayhew, DJ Bozym, C Punckt, IA Aksay, 2010 Acs Nano **4**: 6203.

[8] L Bay, K West, B Winther-Jensen, T Jacobsen, 2006 Sol. Energy Mater. Sol. Cells **90**: 341.

[9] X Zhang, X Chen, K Zhang, S Pang, X Zhou, H Xu, S Dong, P Han, Z Zhang, C Zhang, 2013 Journal of Materials Chemistry A **1**: 3340.

[10] H Xu, X Zhang, C Zhang, Z Liu, X Zhou, S Pang, X Chen, S Dong, Z Zhang, L Zhang, 2012 ACS applied materials & interfaces **4**: 1087.

[11] H Sun, D Qin, S Huang, X Guo, D Li, Y Luo, Q Meng, 2011 Energy & Environmental Science **4**: 2630.

[12] X Xin, M He, W Han, J Jung, Z Lin, 2011 Angew. Chem. Int. Ed. **50**: 11739.

[13] B Chen, S Chang, D Li, L Chen, Y Wang, T Chen, B Zou, H Zhong, AL Rogach, 2015 Chemistry of Materials **27**: 5949.

[14] N Suriyanarayanan, C Mahendran, 2011 Materials Science and Engineering: B **176**: 417.

[15] RK Bhosale, SA Agarkar, I Agrawal, RA Naphade, S Ogale, 2014 RSC Advances **4**: 21989.

[16] L Zhou, X Yang, B Yang, X Zuo, G Li, A Feng, H Tang, H Zhang, M Wu, Y Ma, 2014 J. Power Sources **272**: 639.

[17] M Liu, G Li, X Chen, 2014 ACS applied materials & interfaces **6**: 2604.

[18] CR Dhas, R Venkatesh, DD Kirubakaran, JP Merlin, B Subramanian, AME Raj, 2017 Mater. Chem. Phys. **186**: 561.

[19] C Ravidhas, B Anitha, AME Raj, K Ravichandran, TS Girisun, K Mahalakshmi, K Saravanakumar, C Sanjeeviraja, 2015 Journal of Materials Science: Materials in Electronics **26**: 3573.

[20] V Gowthami, M Meenakshi, P Perumal, R Sivakuma, C Sanjeeviraja, 2014 Mater. Sci. Semicond. Process. **27**: 1042.

[21] AME Raj, SG Victoria, VB Jothy, C Ravidhas, J Wollschläger, M Suendorf, M Neumann, M Jayachandran, C Sanjeeviraja, 2010 Appl. Surf. Sci. **256**: 2920.

[22] P Rajkumar, K Ravichandran, M Baneto, C Ravidhas, B Sakthivel, N Dineshbabu, 2015 Mater. Sci. Semicond. Process. **35**: 189.

[23] M-S Fan, J-H Chen, C-T Li, K-W Cheng, K-C Ho, 2015 Journal of Materials Chemistry A **3**: 562.

[24] CR Dhas, R Venkatesh, R Sivakumar, AME Raj, C Sanjeeviraja, 2017 Opt. Mater. **72**: 717.
[25] C Ravidhas, AJ Josephine, P Sudhagar, A Devadoss, C Terashima, K Nakata, A Fujishima, AME Raj, C Sanjeeviraja, 2015 Mater. Sci. Semicond. Process. **30**: 343.
[26] TP Rao, M Santhoshkumar, 2009 Appl. Surf. Sci. **255**: 4579.
[27] J Lodder, T Wielinga, J Worst, 1983 Thin Solid Films **101**: 61.
[28] R Swapna, M Ashok, G Muralidharan, MS Kumar, 2013 J. Anal. Appl. Pyrolysis **102**: 68.
[29] CR Dhas, AJ Christy, R Venkatesh, B Anitha, AJ Josephine, DD Kirubakaran, D Arivukarasan, P Sudhagar, AME Raj, C Sanjeeviraja, 2017 Recent Trends in Materials Science and Applications **189**: 451.
[30] A Jeong, W Jo, M Song, S Yoon, 2012 Mater. Chem. Phys. **134**: 1030.
[31] J Chang, H Kuo, I Leu, M Hon, 2002 Sensors and actuators B: Chemical **84**: 258.
[32] B Anitha, C Ravidhas, R Venkatesh, AME Raj, K Ravichandran, B Subramanian, C Sanjeeviraja, 2017 Physica E: Low-dimensional Systems and Nanostructures **91**: 148.
[33] M Baneto, A Enesca, C Mihoreanu, Y Lare, K Jondo, K Napo, A Duta, 2015 Ceram. Int. **41**: 4742.
[34] A Moholkar, S Shinde, A Babar, K-U Sim, HK Lee, K Rajpure, P Patil, C Bhosale, J Kim, 2011 J. Alloys Compd. **509**: 7439.
[35] PJ ávan der Put, 1996 J. Mater. Chem. **6**: 765.
[36] TT John, T Sebastian, CS Kartha, K Vijayakumar, T Abe, Y Kashiwaba, 2007 Physica B: Condensed Matter **388**: 1.
[37] M Zouaghi, TB Nasrallah, S Marsillac, J Bernede, S Belgacem, 2001 Thin Solid Films **382**: 39.
[38] SD Perera, H Zhang, X Ding, A Nelson, RD Robinson, 2015 Journal of Materials Chemistry C **3**: 1044.
[39] A Katerski, A Mere, V Kazlauskiene, J Miskinis, A Saar, L Matisen, A Kikas, M Krunks, 2008 Thin Solid Films **516**: 7110.
[40] ND Sankir, E Aydin, H Unver, E Uluer, M Parlak, 2013 Solar Energy **95**: 21.
[41] J Qiu, Z Jin, J Qian, Y Shi, W Wu, 2005 J. Cryst. Growth **282**: 421.
[42] C-S Cheng, M Serizawa, H Sakata, T Hirayama, 1998 Mater. Chem. Phys. **53**: 225.
[43] M Yakushev, R Martin, A Mudryi, A Ivaniukovich, 2008 Appl. Phys. Lett. **92**: 111908.
[44] M Sahal, B Marí, M Mollar, 2009 Thin Solid Films **517**: 2202.
[45] C Ravi Dhas, AJ Christy, R Venkatesh, DD Kirubakaran, R Sivakumar, K Ravichandran, AME Raj, C Sanjeeviraja, 2016 Mater. Res. Innovations: 1.
[46] J Kong, Z-J Zhou, M Li, W-H Zhou, S-J Yuan, R-Y Yao, Y Zhao, S-X Wu, 2013 Nanoscale research letters **8**: 464.
[47] K Mokurala, S Mallick, 2017 RSC Advances **7**: 15139.
[48] CV Gopi, SS Rao, S-K Kim, D Punnoose, H-J Kim, 2015 J. Power Sources **275**: 547.
[49] S-L Chen, A-C Xu, J Tao, H-J Tao, Y-Z Shen, L-M Zhu, J-J Jiang, T Wang, L Pan, 2016 Green Chemistry **18**: 2793.
[50] Z Zhang, S Pang, H Xu, Z Yang, X Zhang, Z Liu, X Wang, X Zhou, S Dong, X Chen, 2013 RSC Advances **3**: 16528.

**Table 1: Root Mean Square Roughness and Activation Energy of CIS thin films**

| Solvent Volume (ml) | Root Mean Square Roughness (nm) | Activation Energy (eV) | |
|---|---|---|---|
| | | $E_aI$ | $E_aII$ |
| 10 | 24 | 0.65 | 0.42 |
| 30 | 21 | 0.48 | 0.36 |
| 50 | 15 | 0.40 | 0.34 |
| 70 | 23 | 0.35 | 0.55 |

**Table 2: Electrochemical parameters of DSSCs for different CEs**

| Samples | $J_{pa}$ ($mA/cm^2$) | $J_{pc}$ ($mA/cm^2$) | $\Delta E_p$ (mV) | $R_s$ ($\Omega\ cm^2$) | $R_{ct}$ ($\Omega\ cm^2$) | log $J_{lim}$ ($mA/cm^2$) |
|---|---|---|---|---|---|---|
| Pt | 1.75 | -1.00 | 421 | 5.12 | 2.46 | 7.14 |
| 10 ml | 0.93 | -0.50 | 471 | 7.56 | 95.53 | 2.74 |
| 30 ml | 1.01 | -0.41 | 450 | 6.99 | 90.06 | 5.29 |
| 50 ml | 1.72 | -0.58 | 425 | 6.44 | 57.10 | 6.96 |
| 70 ml | 1.03 | -0.45 | 432 | 7.10 | 87.81 | 6.27 |

**Table 3: Photocurrent density-voltage (J-V) parameters of DSSCs for different CEs**

| Samples | $V_{oc}$ (V) | $J_{sc}$ (mA/cm$^2$) | FF | η (%) |
|---|---|---|---|---|
| Pt | 0.78 | 10.87 | 0.63 | 5.30 |
| 10 ml | 0.76 | 4.55 | 0.33 | 1.13 |
| 30 ml | 0.76 | 6.45 | 0.35 | 1.72 |
| 50 ml | 0.77 | 9.21 | 0.46 | 3.25 |
| 70 ml | 0.75 | 7.43 | 0.45 | 2.52 |

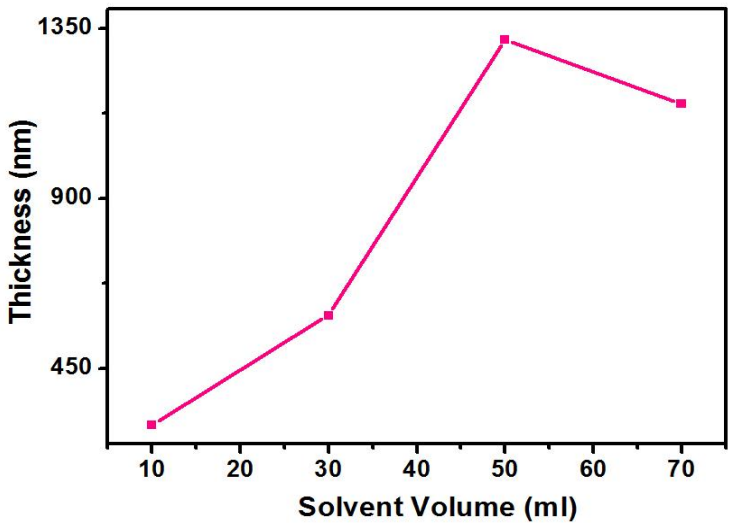


**Figure 1: Solvent volume vs thickness of CIS thin films**

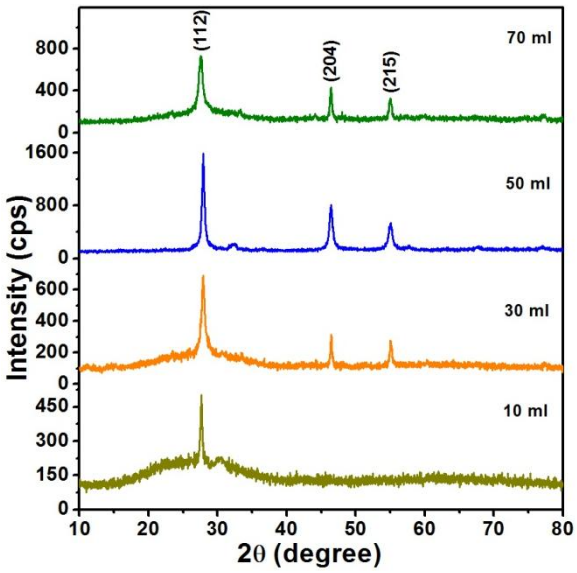


**Figure 2: X-ray diffraction of CIS thin films for different solvent volumes**

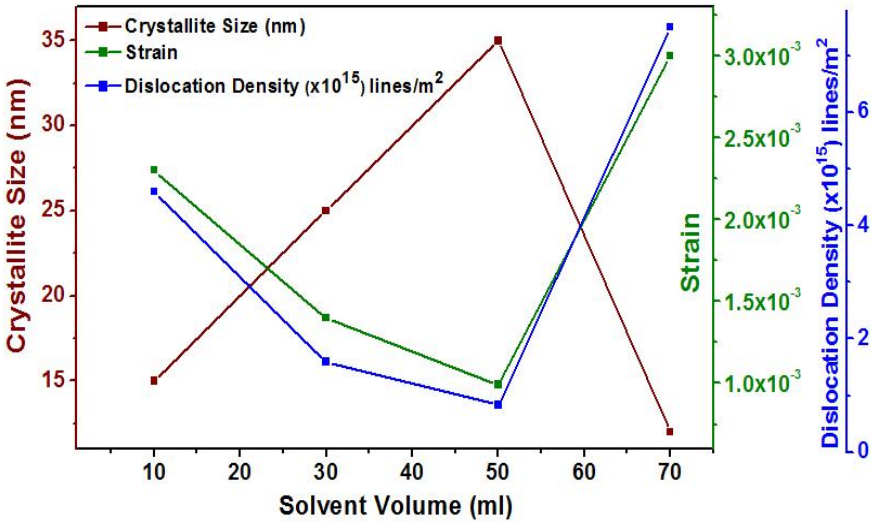


**Figure 3: Solvent volume vs crystallite size, strain and dislocation density of CIS thin films**

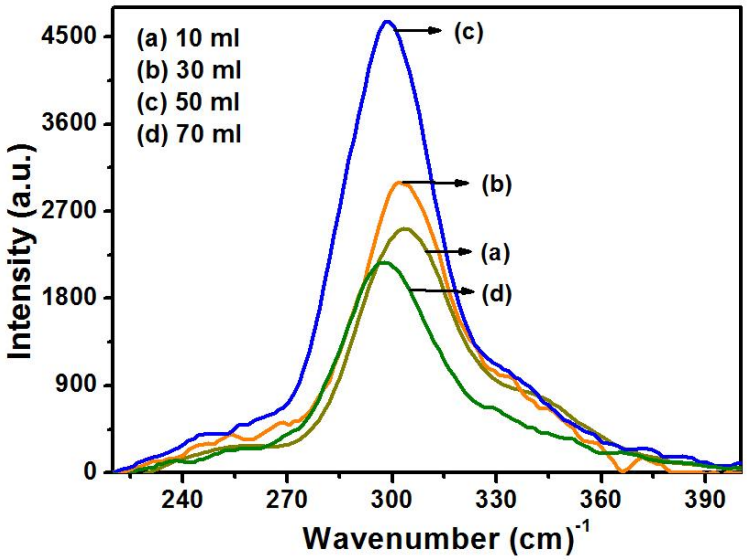


**Figure 4: Raman Spectra of CIS thin films for different solvent volumes**

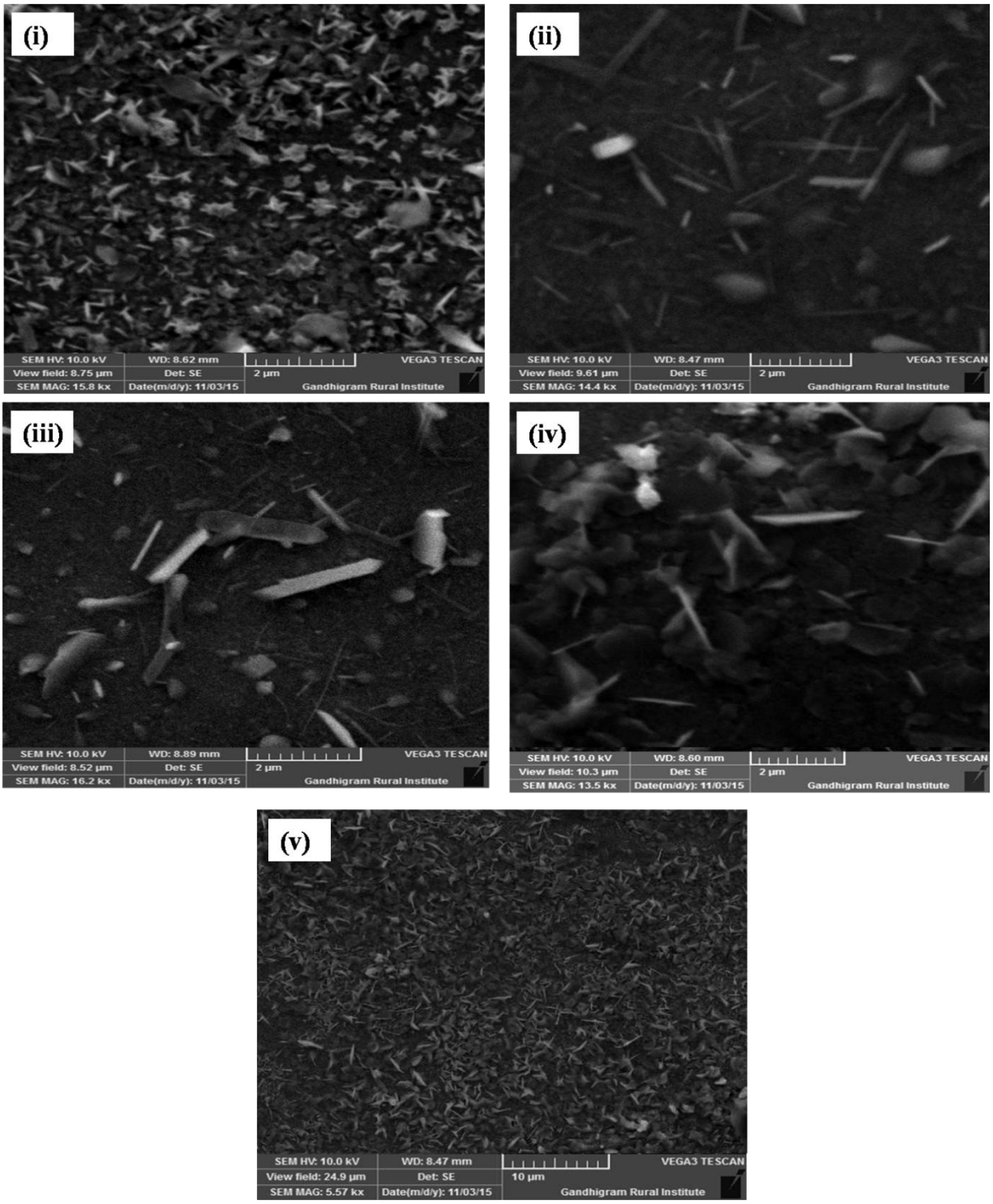


**Figure 5: SEM images of CIS thin films (i) 10 ml (ii) 30 ml (iii) 50 ml (iv) 70 ml and (v) 50 ml higher magnification**

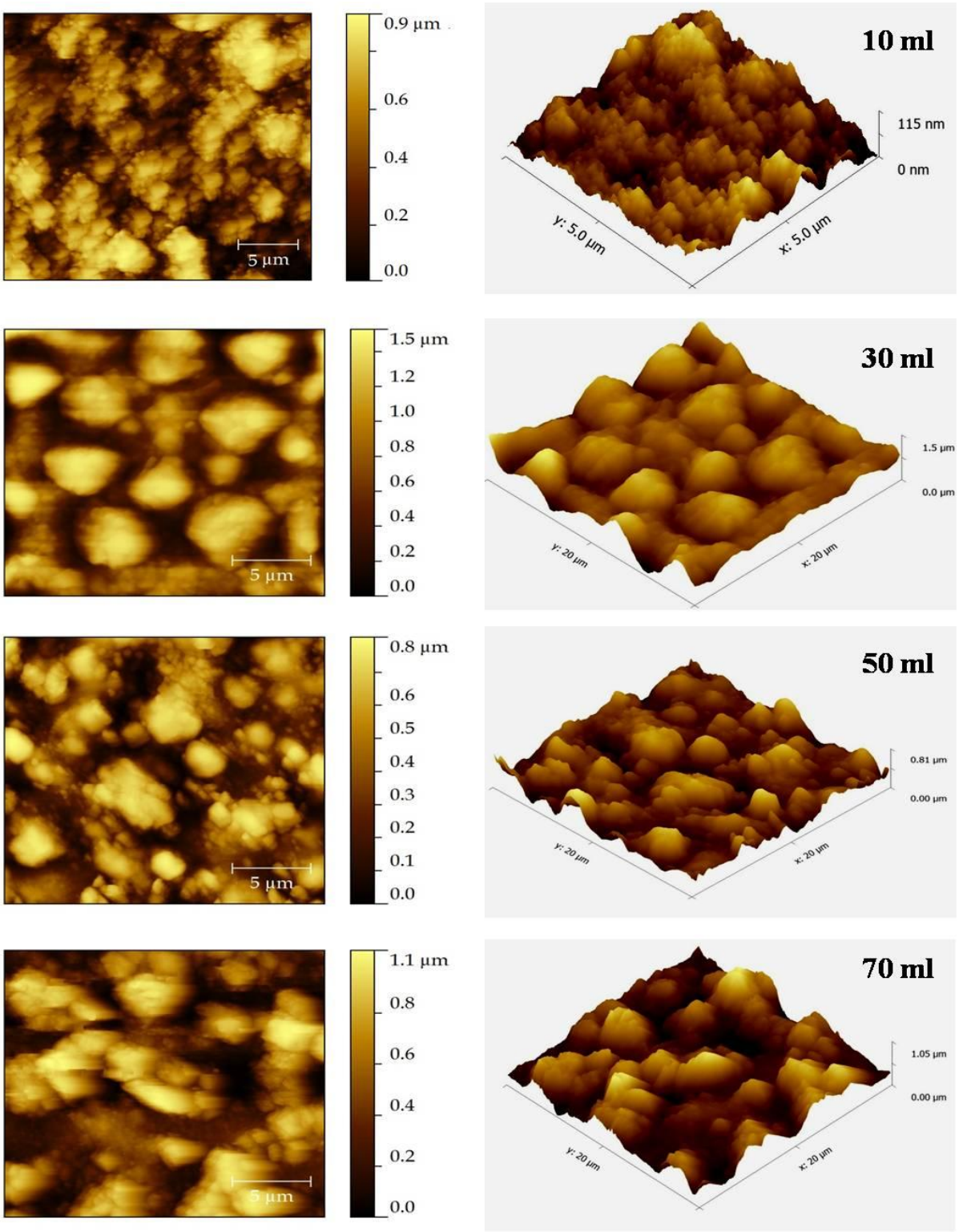


**Figure 6: AFM images of CIS thin films for different solvent volumes**

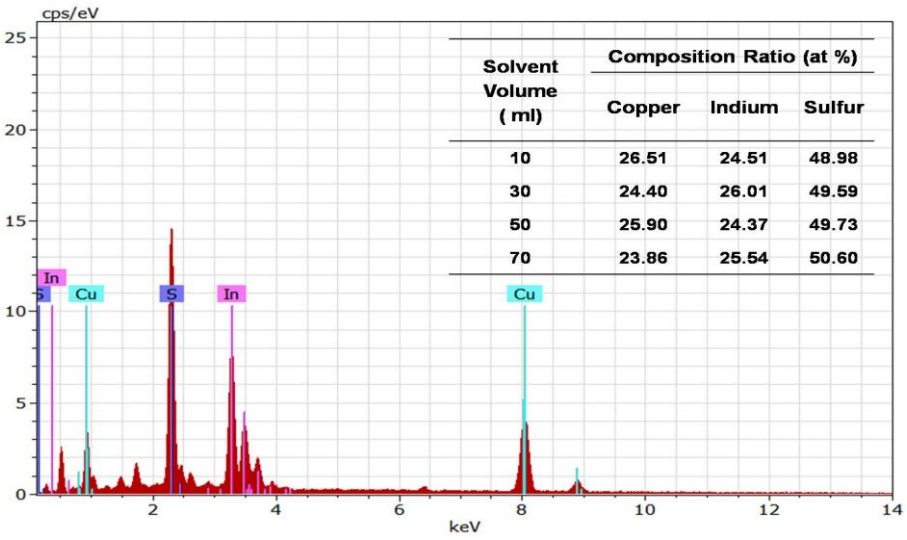


| Solvent Volume ( ml) | Composition Ratio (at %) | | |
|---|---|---|---|
| | Copper | Indium | Sulfur |
| 10 | 26.51 | 24.51 | 48.98 |
| 30 | 24.40 | 26.01 | 49.59 |
| 50 | 25.90 | 24.37 | 49.73 |
| 70 | 23.86 | 25.54 | 50.60 |

**Figure 7: EDS analysis of CIS thin film**

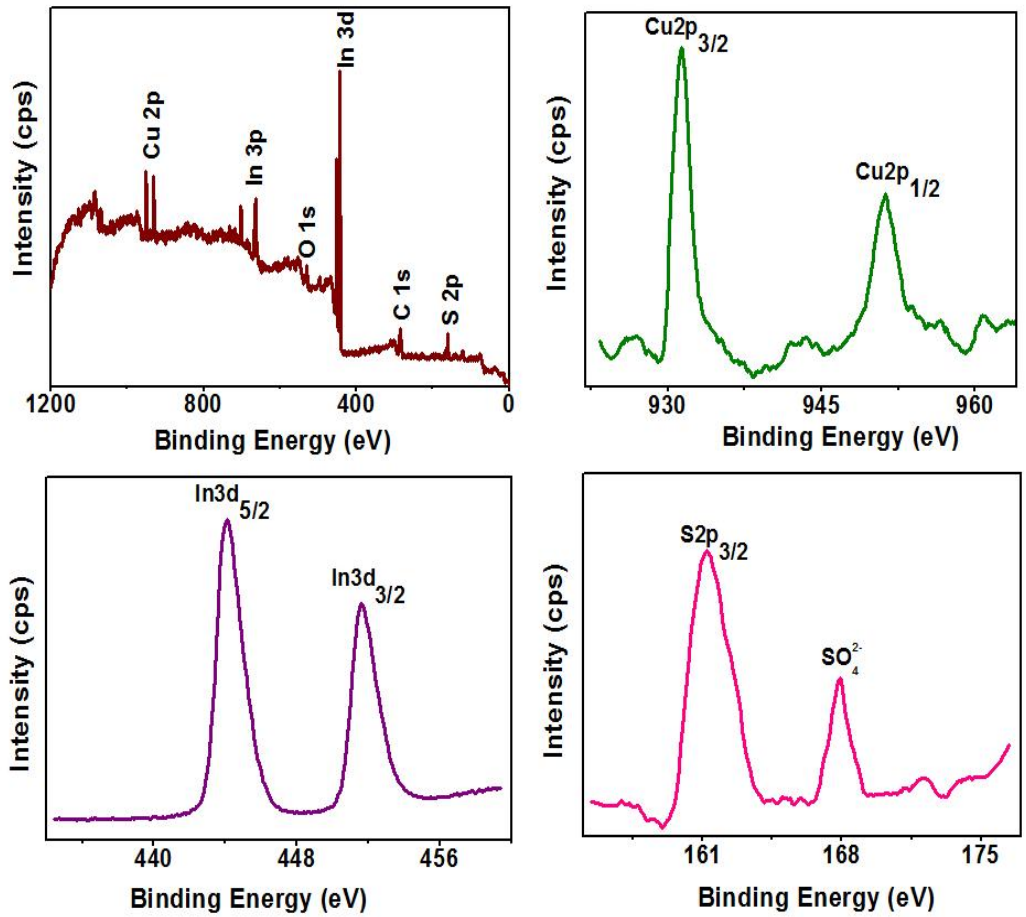


**Figure 8: Survey spectrum and Core level spectra of Cu, In and S of CIS thin film deposited for the solvent volume of 50 ml**

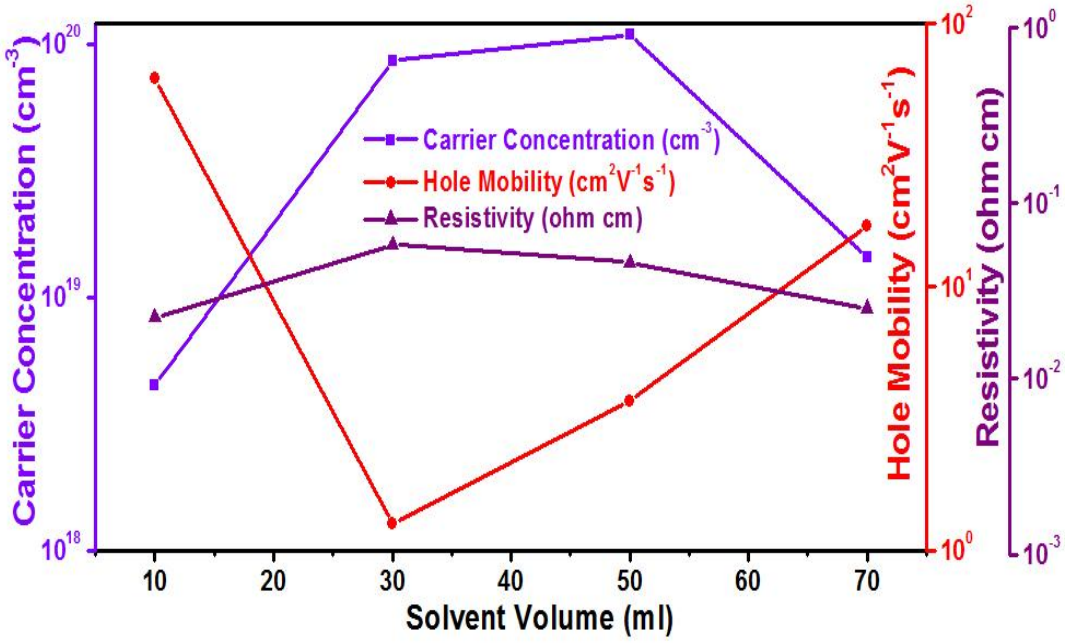


**Figure 9: Electrical parameters of CIS thin films deposited for different solvent volumes**

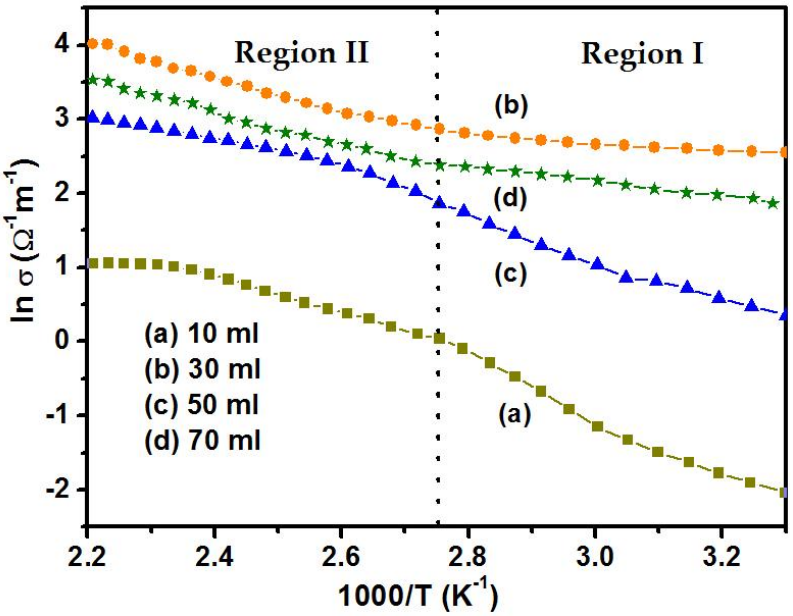


**Figure 10: Arrhenius plot (ln σ vs. 1000/T ($K^{-1}$)) of CIS films for different solvent volumes**

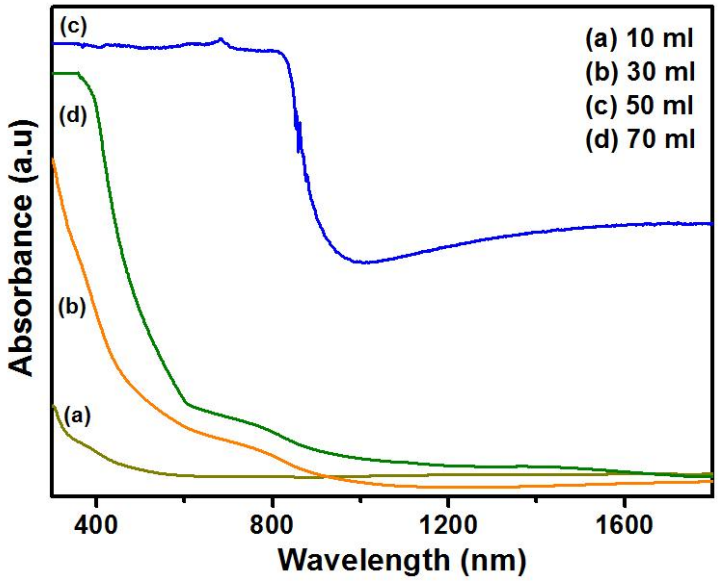


**Figure 11: Absorbance vs wavelength of CIS thin films for different solvent volumes**

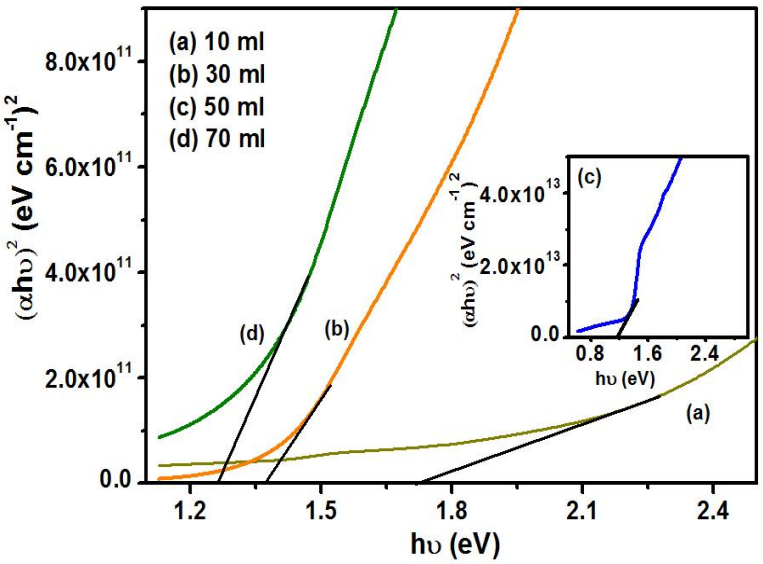


**Figure 12: Optical band gap of CIS thin films for different solvent volumes**

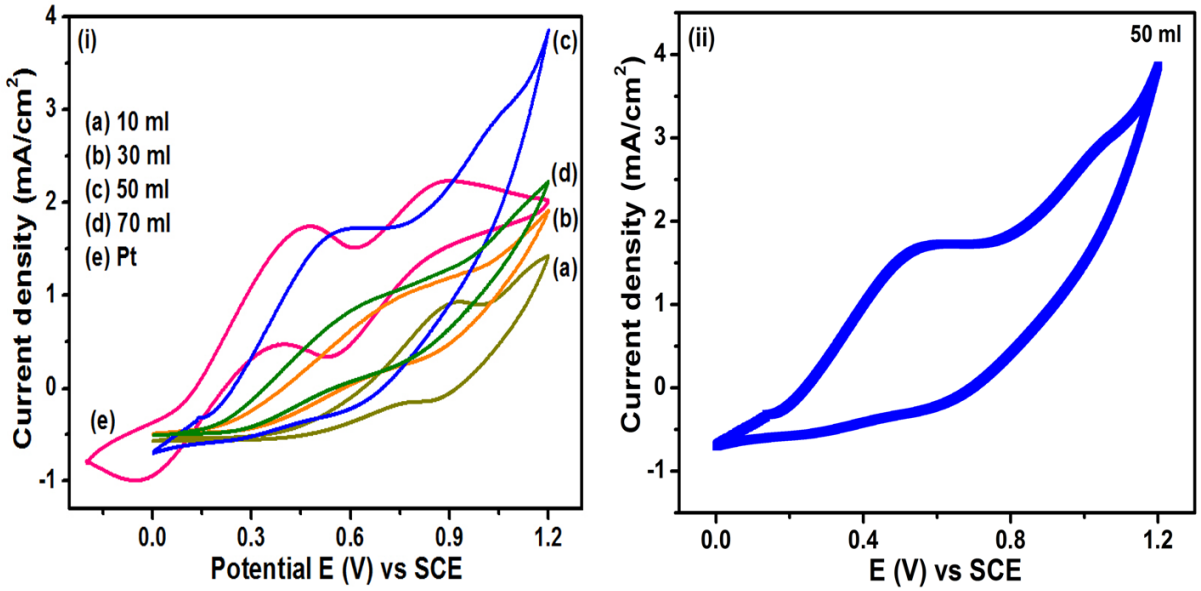


**Figure 13: (i) Cyclic voltammograms of Pt and CIS CEs and (ii) 40 continuous cyclic voltammograms of CIS CE deposited for 50 ml**

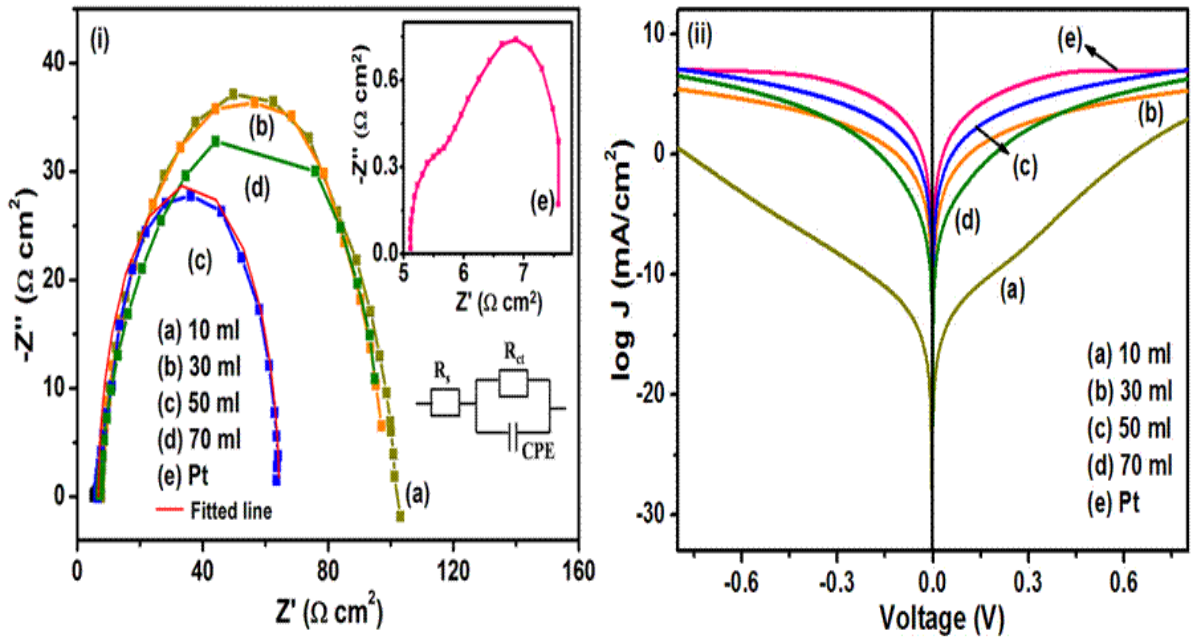


**Figure 14: (i) EIS spectra of the $TiO_2$ based DSSCs devices with Pt and CIS CEs and (ii) Tafel polarization curves of Pt and CIS symmetric cells**

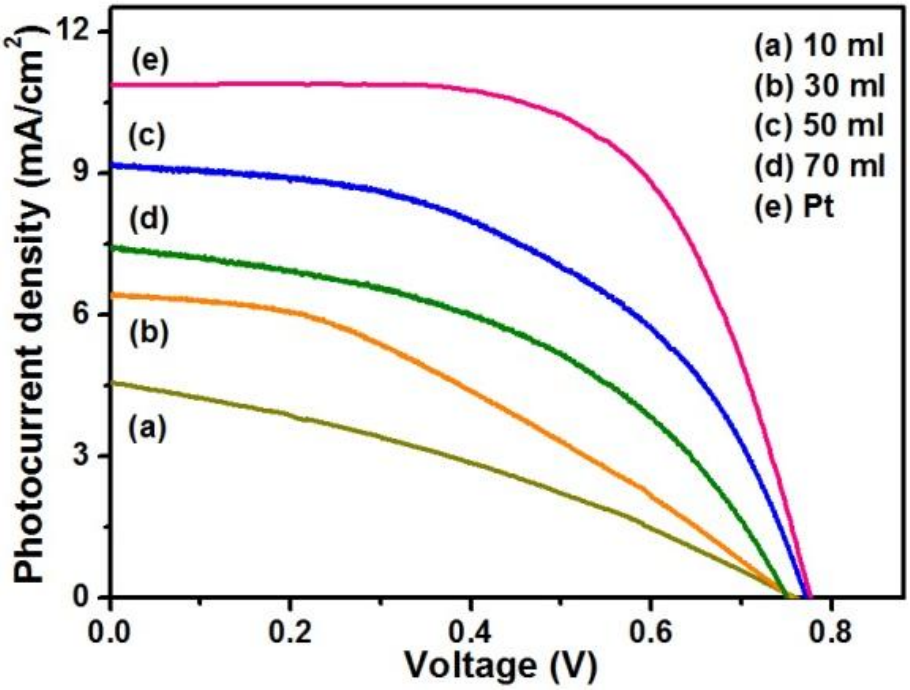


**Figure 15: J – V characteristics of DSSCs with Pt and different CIS CEs**